Measurement of the ratio of inclusive cross sections $\sigma(p\bar{p} \to Z + 2b \text{ jets})/\sigma(p\bar{p} \to Z + 2 \text{ jets})$ in $p\bar{p}$ collisions at $\sqrt{s} = 1.96$ TeV

V. M. Abazov,[31] B. Abbott,[67] B. S. Acharya,[25] M. Adams,[46] T. Adams,[44] J. P. Agnew,[41] G. D. Alexeev,[31] G. Alkhazov,[35] A. Alton,[56,a] A. Askew,[44] S. Atkins,[54] K. Augsten,[7] C. Avila,[5] F. Badaud,[10] L. Bagby,[45] B. Baldin,[45] D. V. Bandurin,[73] S. Banerjee,[25] E. Barberis,[55] P. Baringer,[53] J. F. Bartlett,[45] U. Bassler,[15] V. Bazterra,[46] A. Bean,[53] M. Begalli,[2] L. Bellantoni,[45] S. B. Beri,[23] G. Bernardi,[14] R. Bernhard,[19] I. Bertram,[39] M. Besançon,[15] R. Beuselinck,[40] P. C. Bhat,[45] S. Bhatia,[58] V. Bhatnagar,[23] G. Blazey,[47] S. Blessing,[44] K. Bloom,[59] A. Boehnlein,[45] D. Boline,[64] E. E. Boos,[33] G. Borissov,[39] M. Borysova,[38,l] A. Brandt,[70] O. Brandt,[20] R. Brock,[57] A. Bross,[45] D. Brown,[14] X. B. Bu,[45] M. Buehler,[45] V. Buescher,[21] V. Bunichev,[33] S. Burdin,[39,b] C. P. Buszello,[37] E. Camacho-Pérez,[28] B. C. K. Casey,[45] H. Castilla-Valdez,[28] S. Caughron,[57] S. Chakrabarti,[64] K. M. Chan,[51] A. Chandra,[72] E. Chapon,[15] G. Chen,[53] S. W. Cho,[27] S. Choi,[27] B. Choudhary,[24] S. Cihangir,[45] D. Claes,[59] J. Clutter,[53] M. Cooke,[45,k] W. E. Cooper,[45] M. Corcoran,[72] F. Couderc,[15] M.-C. Cousinou,[12] D. Cutts,[69] A. Das,[71] G. Davies,[40] S. J. de Jong,[29,30] E. De La Cruz-Burelo,[28] F. Déliot,[15] R. Demina,[63] D. Denisov,[45] S. P. Denisov,[34] S. Desai,[45] C. Deterre,[41,c] K. DeVaughan,[59] H. T. Diehl,[45] M. Diesburg,[45] P. F. Ding,[41] A. Dominguez,[59] A. Dubey,[24] L. V. Dudko,[33] A. Duperrin,[12] S. Dutt,[23] M. Eads,[47] D. Edmunds,[57] J. Ellison,[43] V. D. Elvira,[45] Y. Enari,[14] H. Evans,[49] V. N. Evdokimov,[34] A. Fauré,[15] L. Feng,[47] T. Ferbel,[63] F. Fiedler,[21] F. Filthaut,[29,30] W. Fisher,[57] H. E. Fisk,[45] M. Fortner,[47] H. Fox,[39] S. Fuess,[45] P. H. Garbincius,[45] A. Garcia-Bellido,[63] J. A. García-González,[28] V. Gavrilov,[32] W. Geng,[12,57] C. E. Gerber,[46] Y. Gershtein,[60] G. Ginther,[45,63] O. Gogota,[38] G. Golovanov,[31] P. D. Grannis,[64] S. Greder,[16] H. Greenlee,[45] G. Grenier,[17] Ph. Gris,[10] J.-F. Grivaz,[13] A. Grohsjean,[15,c] S. Grünendahl,[45] M. W. Grünewald,[26] T. Guillemin,[13] G. Gutierrez,[45] P. Gutierrez,[67] J. Haley,[68] L. Han,[4] K. Harder,[41] A. Harel,[63] J. M. Hauptman,[52] J. Hays,[40] T. Head,[41] T. Hebbeker,[18] D. Hedin,[47] H. Hegab,[68] A. P. Heinson,[43] U. Heintz,[69] C. Hensel,[1] I. Heredia-De La Cruz,[28,d] K. Herner,[45] G. Hesketh,[41,f] M. D. Hildreth,[51] R. Hirosky,[73] T. Hoang,[44] J. D. Hobbs,[64] B. Hoeneisen,[9] J. Hogan,[72] M. Hohlfeld,[21] J. L. Holzbauer,[58] I. Howley,[70] Z. Hubacek,[7,15] V. Hynek,[7] I. Iashvili,[62] Y. Ilchenko,[71] R. Illingworth,[45] A. S. Ito,[45] S. Jabeen,[45,m] M. Jaffré,[13] A. Jayasinghe,[67] M. S. Jeong,[27] R. Jesik,[40] P. Jiang,[4] K. Johns,[42] E. Johnson,[57] M. Johnson,[45] A. Jonckheere,[45] P. Jonsson,[40] J. Joshi,[43] A. W. Jung,[45] A. Juste,[36] E. Kajfasz,[12] D. Karmanov,[33] I. Katsanos,[59] M. Kaur,[23] R. Kehoe,[71] S. Kermiche,[12] N. Khalatyan,[45] A. Khanov,[68] A. Kharchilava,[62] Y. N. Kharzheev,[31] I. Kiselevich,[32] J. M. Kohli,[23] A. V. Kozelov,[34] J. Kraus,[58] A. Kumar,[62] A. Kupco,[8] T. Kurča,[17] V. A. Kuzmin,[33] S. Lammers,[49] P. Lebrun,[17] H. S. Lee,[27] S. W. Lee,[52] W. M. Lee,[45] X. Lei,[42] J. Lellouch,[14] D. Li,[14] H. Li,[73] L. Li,[43] Q. Z. Li,[45] J. K. Lim,[27] D. Lincoln,[45] J. Linnemann,[57] V. V. Lipaev,[34] R. Lipton,[45] H. Liu,[71] Y. Liu,[4] A. Lobodenko,[35] M. Lokajicek,[8] R. Lopes de Sa,[45] R. Luna-Garcia,[28,g] A. L. Lyon,[45] A. K. A. Maciel,[1] R. Madar,[19] R. Magaña-Villalba,[28] S. Malik,[59] V. L. Malyshev,[31] J. Mansour,[20] J. Martínez-Ortega,[28] R. McCarthy,[64] C. L. McGivern,[41] M. M. Meijer,[29,30] A. Melnitchouk,[45] D. Menezes,[47] P. G. Mercadante,[3] M. Merkin,[33] A. Meyer,[18] J. Meyer,[20,i] F. Miconi,[16] N. K. Mondal,[25] M. Mulhearn,[73] E. Nagy,[12] M. Narain,[69] R. Nayyar,[42] H. A. Neal,[56] J. P. Negret,[5] P. Neustroev,[35] H. T. Nguyen,[73] T. Nunnemann,[22] J. Orduna,[72] N. Osman,[12] J. Osta,[51] A. Pal,[70] N. Parashar,[50] V. Parihar,[69] S. K. Park,[27] R. Partridge,[69,e] N. Parua,[49] A. Patwa,[65,j] B. Penning,[45] M. Perfilov,[33] Y. Peters,[41] K. Petridis,[41] G. Petrillo,[63] P. Pétroff,[13] M.-A. Pleier,[65] V. M. Podstavkov,[45] A. V. Popov,[34] M. Prewitt,[72] D. Price,[41] N. Prokopenko,[34] J. Qian,[56] A. Quadt,[20] B. Quinn,[58] P. N. Ratoff,[39] I. Razumov,[34] I. Ripp-Baudot,[16] F. Rizatdinova,[68] M. Rominsky,[45] A. Ross,[39] C. Royon,[15] P. Rubinov,[45] R. Ruchti,[51] G. Sajot,[11] A. Sánchez-Hernández,[28] M. P. Sanders,[22] A. S. Santos,[1,h] G. Savage,[45] M. Savitskyi,[38] L. Sawyer,[54] T. Scanlon,[40] R. D. Schamberger,[64] Y. Scheglov,[35] H. Schellman,[48] C. Schwanenberger,[41] R. Schwienhorst,[57] J. Sekaric,[53] H. Severini,[67] E. Shabalina,[20] V. Shary,[15] S. Shaw,[41] A. A. Shchukin,[34] V. Simak,[7] P. Skubic,[67] P. Slattery,[63] D. Smirnov,[51] G. R. Snow,[59] J. Snow,[66] S. Snyder,[65] S. Söldner-Rembold,[41] L. Sonnenschein,[18] K. Soustruznik,[6] J. Stark,[11] D. A. Stoyanova,[34] M. Strauss,[67] L. Suter,[41] P. Svoisky,[67] M. Titov,[15] V. V. Tokmenin,[31] Y.-T. Tsai,[63] D. Tsybychev,[64] B. Tuchming,[15] C. Tully,[61] L. Uvarov,[35] S. Uvarov,[35] S. Uzunyan,[47] R. Van Kooten,[49] W. M. van Leeuwen,[29] N. Varelas,[46] E. W. Varnes,[42] I. A. Vasilyev,[34] A. Y. Verkheev,[31] L. S. Vertogradov,[31] M. Verzocchi,[45] M. Vesterinen,[41] D. Vilanova,[15] P. Vokac,[7] H. D. Wahl,[44] M. H. L. S. Wang,[45] J. Warchol,[51] G. Watts,[74] M. Wayne,[51] J. Weichert,[21] L. Welty-Rieger,[48] M. R. J. Williams,[49,n] G. W. Wilson,[53] M. Wobisch,[54] D. R. Wood,[55] T. R. Wyatt,[41] Y. Xie,[45] R. Yamada,[45] S. Yang,[4] T. Yasuda,[45] Y. A. Yatsunenko,[31] W. Ye,[64] Z. Ye,[45] H. Yin,[45] K. Yip,[65] S. W. Youn,[45] J. M. Yu,[56] J. Zennamo,[62] T. G. Zhao,[41] B. Zhou,[56] J. Zhu,[56] M. Zielinski,[63] D. Zieminska,[49] and L. Zivkovic[14]

(D0 Collaboration)

[1]*LAFEX, Centro Brasileiro de Pesquisas Físicas, Rio de Janeiro, Brazil*
[2]*Universidade do Estado do Rio de Janeiro, Rio de Janeiro, Brazil*
[3]*Universidade Federal do ABC, Santo André, Brazil*
[4]*University of Science and Technology of China, Hefei, People's Republic of China*
[5]*Universidad de los Andes, Bogotá, Colombia*

[6]*Charles University, Faculty of Mathematics and Physics, Center for Particle Physics, Prague, Czech Republic*
[7]*Czech Technical University in Prague, Prague, Czech Republic*
[8]*Institute of Physics, Academy of Sciences of the Czech Republic, Prague, Czech Republic*
[9]*Universidad San Francisco de Quito, Quito, Ecuador*
[10]*LPC, Université Blaise Pascal, CNRS/IN2P3, Clermont, France*
[11]*LPSC, Université Joseph Fourier Grenoble 1, CNRS/IN2P3, Institut National Polytechnique de Grenoble, Grenoble, France*
[12]*CPPM, Aix-Marseille Université, CNRS/IN2P3, Marseille, France*
[13]*LAL, Université Paris-Sud, CNRS/IN2P3, Orsay, France*
[14]*LPNHE, Universités Paris VI and VII, CNRS/IN2P3, Paris, France*
[15]*CEA, Irfu, SPP, Saclay, France*
[16]*IPHC, Université de Strasbourg, CNRS/IN2P3, Strasbourg, France*
[17]*IPNL, Université Lyon 1, CNRS/IN2P3, Villeurbanne, France and Université de Lyon, Lyon, France*
[18]*III. Physikalisches Institut A, RWTH Aachen University, Aachen, Germany*
[19]*Physikalisches Institut, Universität Freiburg, Freiburg, Germany*
[20]*II. Physikalisches Institut, Georg-August-Universität Göttingen, Göttingen, Germany*
[21]*Institut für Physik, Universität Mainz, Mainz, Germany*
[22]*Ludwig-Maximilians-Universität München, München, Germany*
[23]*Panjab University, Chandigarh, India*
[24]*Delhi University, Delhi, India*
[25]*Tata Institute of Fundamental Research, Mumbai, India*
[26]*University College Dublin, Dublin, Ireland*
[27]*Korea Detector Laboratory, Korea University, Seoul, Korea*
[28]*CINVESTAV, Mexico City, Mexico*
[29]*Nikhef, Science Park, Amsterdam, The Netherlands*
[30]*Radboud University Nijmegen, Nijmegen, The Netherlands*
[31]*Joint Institute for Nuclear Research, Dubna, Russia*
[32]*Institute for Theoretical and Experimental Physics, Moscow, Russia*
[33]*Moscow State University, Moscow, Russia*
[34]*Institute for High Energy Physics, Protvino, Russia*
[35]*Petersburg Nuclear Physics Institute, St. Petersburg, Russia*
[36]*Institució Catalana de Recerca i Estudis Avançats (ICREA) and Institut de Física d'Altes Energies (IFAE), Barcelona, Spain*
[37]*Uppsala University, Uppsala, Sweden*
[38]*Taras Shevchenko National University of Kyiv, Kiev, Ukraine*
[39]*Lancaster University, Lancaster LA1 4YB, United Kingdom*
[40]*Imperial College London, London SW7 2AZ, United Kingdom*
[41]*The University of Manchester, Manchester M13 9PL, United Kingdom*
[42]*University of Arizona, Tucson, Arizona 85721, USA*
[43]*University of California Riverside, Riverside, California 92521, USA*
[44]*Florida State University, Tallahassee, Florida 32306, USA*
[45]*Fermi National Accelerator Laboratory, Batavia, Illinois 60510, USA*
[46]*University of Illinois at Chicago, Chicago, Illinois 60607, USA*
[47]*Northern Illinois University, DeKalb, Illinois 60115, USA*
[48]*Northwestern University, Evanston, Illinois 60208, USA*
[49]*Indiana University, Bloomington, Indiana 47405, USA*
[50]*Purdue University Calumet, Hammond, Indiana 46323, USA*
[51]*University of Notre Dame, Notre Dame, Indiana 46556, USA*
[52]*Iowa State University, Ames, Iowa 50011, USA*
[53]*University of Kansas, Lawrence, Kansas 66045, USA*
[54]*Louisiana Tech University, Ruston, Louisiana 71272, USA*
[55]*Northeastern University, Boston, Massachusetts 02115, USA*
[56]*University of Michigan, Ann Arbor, Michigan 48109, USA*
[57]*Michigan State University, East Lansing, Michigan 48824, USA*
[58]*University of Mississippi, University, Mississippi 38677, USA*
[59]*University of Nebraska, Lincoln, Nebraska 68588, USA*
[60]*Rutgers University, Piscataway, New Jersey 08855, USA*
[61]*Princeton University, Princeton, New Jersey 08544, USA*
[62]*State University of New York, Buffalo, New York 14260, USA*

[63]University of Rochester, Rochester, New York 14627, USA
[64]State University of New York, Stony Brook, New York 11794, USA
[65]Brookhaven National Laboratory, Upton, New York 11973, USA
[66]Langston University, Langston, Oklahoma 73050, USA
[67]University of Oklahoma, Norman, Oklahoma 73019, USA
[68]Oklahoma State University, Stillwater, Oklahoma 74078, USA
[69]Brown University, Providence, Rhode Island 02912, USA
[70]University of Texas, Arlington, Texas 76019, USA
[71]Southern Methodist University, Dallas, Texas 75275, USA
[72]Rice University, Houston, Texas 77005, USA
[73]University of Virginia, Charlottesville, Virginia 22904, USA
[74]University of Washington, Seattle, Washington 98195, USA

(Received 21 January 2015; published 17 March 2015)

We measure the ratio of cross sections, $\sigma(p\bar{p} \to Z + 2b\,\text{jets})/\sigma(p\bar{p} \to Z + 2\,\text{jets})$, for associated production of a Z boson with at least two jets with transverse momentum $p_T^{\text{jet}} > 20$ GeV and pseudorapidity $|\eta^{\text{jet}}| < 2.5$. This measurement uses data corresponding to an integrated luminosity of 9.7 fb^{-1} collected by the D0 experiment in Run II of Fermilab's Tevatron $p\bar{p}$ Collider at a center-of-mass energy of 1.96 TeV. The measured integrated ratio of $0.0236 \pm 0.0032(\text{stat}) \pm 0.0035(\text{syst})$ is in agreement with predictions from next-to-leading-order perturbative QCD and the Monte Carlo event generators PYTHIA and ALPGEN.

DOI: 10.1103/PhysRevD.91.052010 PACS numbers: 12.38.Qk, 13.85.Qk, 14.65.Fy, 14.70.Hp

Studies of Z boson production in association with a bottom and an antibottom quark provide important tests of the predictions of perturbative quantum chromodynamics (pQCD) [1,2]. A good theoretical description of this process is essential since it forms a major background for a variety of physics processes, including standard model (SM) Higgs boson production in association with a Z boson, $ZH(H \to b\bar{b})$ [3], and searches for supersymmetric partners of the b quark [4].

The ratio of $Z + b$ jet to $Z +$ jet production cross sections, for events with at least one jet, has been previously measured by the CDF [5,6] and D0 [7–9] Collaborations using Run II data. The ATLAS [10] and CMS [11] Collaborations have also studied $Z + b$ jet production at $\sqrt{s} = 7$ TeV.

This article presents the ratio of $Z + 2b$ jets to $Z + 2$ jets inclusive production cross sections and is an extension of the previous D0 measurements utilizing similar event selections. The measurement of the ratio benefits from the cancellation of many systematic uncertainties, such as the uncertainty in luminosity and those related to lepton and jet identification, allowing a more precise comparison with theory. The remaining systematic uncertainties arise from the differences between b jets and light jets. In the following, light-quark flavor (u, d, s) and gluon jets are referred to as "light jets." The $Z + 2b$ jet production cross sections have been measured at CMS [12] and ATLAS [13] at $\sqrt{s} = 7$ TeV. The current measurement is based on the complete Run II data sample collected by the D0 experiment at the Fermilab Tevatron $p\bar{p}$ collider at a center-of-mass energy of $\sqrt{s} = 1.96$ TeV, and corresponds to an integrated luminosity of 9.7 fb^{-1}.

We first briefly describe the main components of the D0 Run II detector [14,15] relevant to this analysis. The D0 detector has a central tracking system consisting of a silicon microstrip tracker (SMT) [16] and a central fiber tracker (CFT), both located within a 1.9 T superconducting solenoidal magnet, with designs optimized for tracking and vertexing at pseudorapidities $|\eta_{\text{det}}| < 3$ and $|\eta_{\text{det}}| < 2.5$, respectively [17]. A liquid argon and uranium calorimeter

[a]Visitor from Augustana College, Sioux Falls, SD, USA.
[b]Visitor from The University of Liverpool, Liverpool, UK.
[c]Visitor from DESY, Hamburg, Germany.
[d]Visitor from Universidad Michoacana de San Nicolas de Hidalgo, Morelia, Mexico.
[e]Visitor from SLAC, Menlo Park, CA, USA.
[f]Visitor from University College London, London, UK.
[g]Visitor from Centro de Investigacion en Computacion-IPN, Mexico City, Mexico.
[h]Visitor from Universidade Estadual Paulista, São Paulo, Brazil.
[i]Visitor from Karlsruher Institut für Technologie (KIT)-Steinbuch Centre for Computing (SCC), D-76128 Karlsruhe, Germany.
[j]Visitor from Office of Science, U.S. Department of Energy, Washington, DC 20585, USA.
[k]Visitor from American Association for the Advancement of Science, Washington, DC 20005, USA.
[l]Visitor from Kiev Institute for Nuclear Research, Kiev, Ukraine.
[m]Visitor from University of Maryland, College Park, MD 20742, USA.
[n]Visitor from European Orgnaization for Nuclear Research (CERN), Geneva, Switzerland.

has a central section (CC) covering pseudorapidities $|\eta_{\rm det}| \lesssim 1.1$, and two end calorimeters (EC) that extend coverage to $|\eta_{\rm det}| \approx 4.2$, with all three housed in separate cryostats [18]. An outer muon system, at $|\eta_{\rm det}| < 2$, consists of a layer of tracking detectors and scintillation counters in front of 1.8 T toroids, followed by two similar layers after the toroids. Luminosity is measured using plastic scintillator arrays located in front of the EC cryostats. The trigger and data acquisition systems are designed to accommodate the high instantaneous luminosities of Run II.

This analysis relies on all components of the D0 detector: tracking systems, the liquid-argon sampling calorimeter, muon system, and the ability to identify secondary vertices [14]. The SMT allows for precise reconstruction of the primary $p\bar{p}$ interaction vertex and secondary vertices [17,19]. It also enables an accurate determination of the impact parameter, defined as the distance of closest approach of a track to the primary interaction vertex in the x-y plane. The impact parameter measurements of tracks, along with reconstructed secondary vertices, are important inputs to the b-jet tagging algorithm.

Events containing Z bosons decaying to $\mu\mu$ or ee are collected using triggers based on single electrons or muons. For the off-line selection requirements discussed below, the triggers have an efficiency of approximately 100% for $Z \to ee$ and more than 78% for $Z \to \mu\mu$ decays depending on the transverse momentum of the muon. The $Z + 2$ jet sample requires the presence of at least two jets in the event, while the $Z + 2b$ jet sample requires at least two b-jet candidates, selected using a b-tagging algorithm [20].

An event is selected if it contains a $p\bar{p}$ interaction vertex, reconstructed from at least three tracks, located within 60 cm of the center of the D0 detector along the beam axis. The selected events must also contain a Z boson candidate with a dilepton invariant mass $70 < M_{\ell\ell} < 110$ GeV.

Dielectron (ee) events are required to have two electrons of transverse momentum (p_T) greater than 15 GeV identified through electromagnetic (EM) showers in the calorimeter. The showers must have more than 97% of their energy deposited in the EM calorimeter, be isolated from other energy depositions, and have transverse and longitudinal energy profiles consistent with that expected for electrons. At least one electron must be identified in the CC, with $|\eta_{\rm det}| < 1.1$, and a second electron either in the CC or the EC, $1.5 < |\eta_{\rm det}| < 2.5$. Electron candidates in the CC are required to match central tracks or have a pattern of hits consistent with the passage of an electron through the central tracker. Electrons in the ECs are not required to have a track matched to them due to deteriorating tracking coverage for $|\eta_{\rm det}| > 2$. Due to the lack of track requirement in EC regions we do not apply any opposite sign requirement for the dielectron events.

The dimuon ($\mu\mu$) event selection requires two oppositely charged muons detected in the muon system that are matched to reconstructed tracks in the central tracker with $p_T > 15$ GeV and $|\eta_{\rm det}| < 2$. These muons must pass a combined tracking and calorimeter isolation requirement discussed in detail in Ref. [3]. Muons originating from cosmic rays are rejected by applying timing criteria using the hits in the scintillation counters and by limiting the measured displacement of the muon track with respect to the $p\bar{p}$ interaction vertex [21].

A total of about 1.2 million Z boson candidate events are retained in the combined ee and $\mu\mu$ channels with the above lepton selection criteria. The $Z + 2$ jet sample is then selected by requiring at least two jets in the event with $p_T^{\rm jet} > 20$ GeV and $|\eta^{\rm jet}| < 2.5$. Jets are reconstructed from energy deposits in the calorimeter using an iterative midpoint cone algorithm [22] with a cone of radius $\Delta R = \sqrt{(\Delta\varphi)^2 + (\Delta y)^2} = 0.5$ where φ is the azimuthal angle and y is the rapidity. Jet energy is corrected for detector response, the presence of noise and multiple $p\bar{p}$ interactions. We also correct the jet energy for the energy of those particles within the reconstruction cone that is deposited in the calorimeter outside the cone (and vice versa) [23].

To suppress background from top-antitop quark ($t\bar{t}$) production, events are rejected if the missing transverse energy is larger than 60 GeV, reducing the $t\bar{t}$ contamination by a factor of two. These selection criteria retain an inclusive sample of 20,950 $Z + 2$ jet event candidates in the combined ee and $\mu\mu$ channels.

Processes such as diboson (WW, WZ, ZZ) production can contribute to the background when two leptons are reconstructed in the final state. Inclusive diboson production is simulated with the PYTHIA [24] Monte Carlo (MC) event generator. The $Z +$ jet, including heavy flavor jets, and $t\bar{t}$ events are modeled by ALPGEN [25], which generates hard subprocesses including higher-order QCD tree-level matrix elements, interfaced with PYTHIA for parton showering and hadronization. The CTEQ6L1 [26] parton distribution functions (PDFs) are used in all simulations. The cross sections of the simulated samples are then scaled to the corresponding higher-order theoretical calculations. For the diboson and $Z + 2$ jet processes, including the $Z + b\bar{b}$ signal process and $Z + c\bar{c}$ production, next-to-leading order (NLO) cross section predictions are taken from MCFM [27]. The $t\bar{t}$ cross section is determined from NLO + NNLL (next-to-next-leading log) calculations [28]. To improve the modeling of the p_T distribution of the Z boson, simulated $Z + 2$ jet events are also reweighted to be consistent with the measured p_T spectrum of Z bosons observed in data [29].

These generated samples are processed through a detailed detector simulation based on GEANT [30]. To model the effects of detector noise and pile-up events, collider data from random beam crossings with the same instantaneous luminosity distribution as for data are superimposed on simulated events. These events are then

reconstructed using the same algorithms as used for data. Scale factors, determined from data using independent samples, are applied to account for differences in reconstruction efficiency between data and simulation. The energies of simulated jets are corrected, based on their flavor, to reproduce the resolution and energy scale observed in data [23].

The background contribution from multijet events, in which jets are misidentified as leptons, is evaluated from data. This is performed using a multijet-enriched sample of events that pass all selection criteria except for some of the lepton quality requirements. In the case of electrons, the multijet sample is obtained by inverting the shower shape requirement and relaxing other electron identification criteria, while for the muon channel, the multijet sample consists of events with muon candidates that fail the isolation requirements. The normalization of the multijet background is determined from a simultaneous fit to the dilepton invariant mass distributions in different jet multiplicity bins.

Figures 1 and 2 show the dilepton invariant mass and leading jet p_T distributions in data compared to the expectations from various processes. The dominant contribution comes from $Z+$ light jet production. The non-$Z+$ jet background fraction in the ee channel is about 15%, and is dominated by multijet production. The muon channel has a higher purity with a background fraction of about 7%.

This analysis employs a two-step procedure to determine the b-quark content of jets in the selected events. First, a b-tagging algorithm is applied to jets to select a sample of $Z+2$ jet events that is enriched in heavy flavor jets. After b tagging, the relative light-, c-, and b-quark content is extracted by fitting templates built from a dedicated

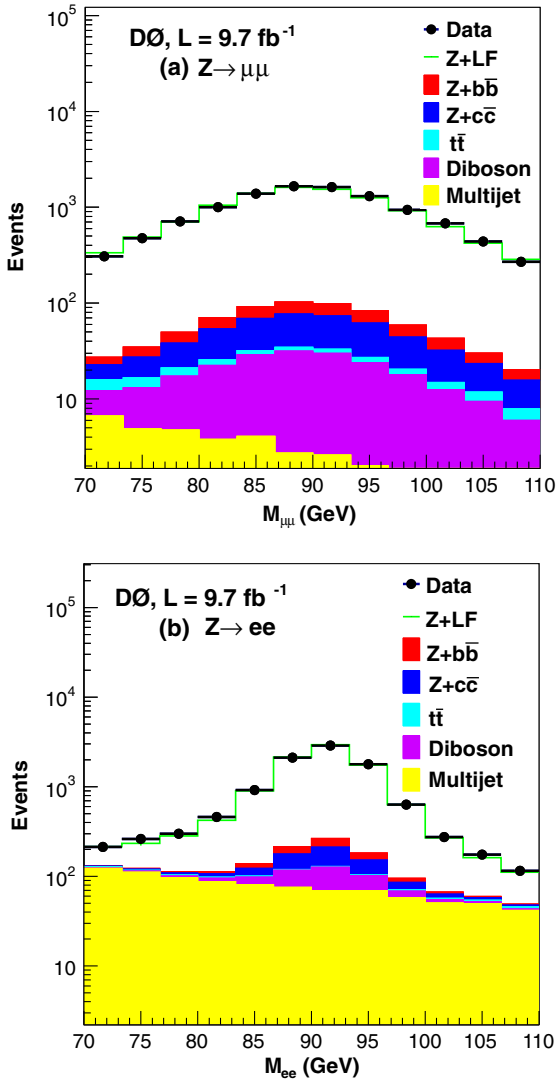

FIG. 1 (color online). The invariant mass in (a) $Z \to \mu\mu$ and (b) $Z \to ee$ channels for data and background in events with a Z boson candidate and at least two jets before b tagging is applied.

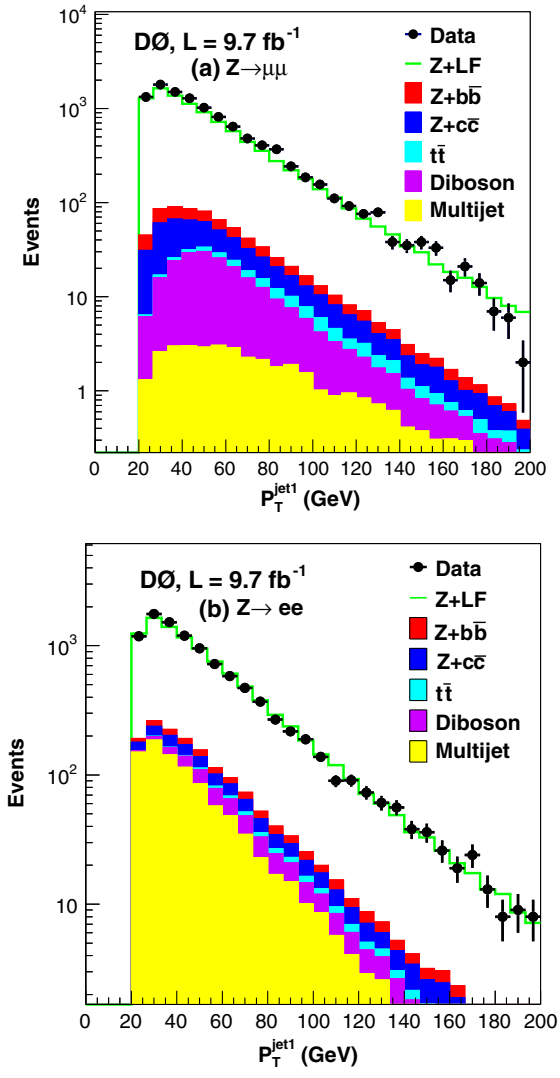

FIG. 2 (color online). The leading jet p_T in the (a) $Z \to \mu\mu$ and (b) $Z \to ee$ channels for data and background in events with a Z boson candidate and at least two jets before b tagging is applied.

discriminant that provides an optimized separation between the three components.

Jets considered for b-jet tagging are subject to a preselection requirement, called taggability, to decouple the intrinsic performance of the b-jet tagging algorithm from effects related to the track reconstruction efficiency. For this purpose, the jet is required to have at least two associated tracks with $p_T > 0.5$ GeV, the leading track must have $p_T > 1$ GeV, and each track must have at least one SMT hit. This requirement has a typical efficiency of 90% per jet.

The b-jet tagging algorithm is based on a multivariate analysis (MVA) technique [31]. This algorithm, MVA$_{bl}$, discriminates b jets from light flavor jets utilizing the relatively long lifetime of the b hadrons when compared to their lighter counterparts [20]. Events with at least two jets tagged by this algorithm are considered.

The MVA$_{bl}$ discriminant combines various properties of the jet and associated tracks to create a continuous output that tends towards unity for b jets and zero for light jets. Inputs include the number of secondary vertices and the charge track multiplicity, invariant mass of the secondary vertex ($M_{\rm SV}$), decay length and impact parameter of secondary vertices, the multiplicity of charged tracks associated with them, and the jet lifetime probability (JLIP), which is the probability that tracks associated with the jet originate from the $p\bar{p}$ interaction vertex [20]. Events are retained for further analysis if they contain at least two jets with an MVA$_{bl}$ output greater than 0.15. After these requirements, 241 $Z + 2$ jet events are selected with at least two b-tagged jets, where only the two highest p_T tagged jets are examined in the analysis and the electron and muon channels are combined. The efficiency for tagging two b jets in data is 33%. In the MC correction, factors are applied to account for differences with data [20]. The background contamination from diboson, multijet, and top production after b-tagging, for the electron and muon channels combined are 8%, 2% and 15%, respectively.

To determine the fraction of events with $2b$ jets, a dedicated discriminant, $D_{\rm MJL}$, is employed [8,32]. It is a combination of the two most discriminating MVA$_{bl}$ inputs, $M_{\rm SV}$ and JLIP: $D_{\rm MJL} = 0.5 \times (M_{\rm SV}/(5\ {\rm GeV}) - \ln({\rm JLIP})/20)$.

To measure the fraction of events with different jet flavors in the selected sample, we count the number of events as a function of the $D_{\rm MJL}$ of the two leading jets $N(D_{{\rm MJL}_1}, D_{{\rm MJL}_2})$ and then perform a two-dimensional binned maximum likelihood fit to that distribution. The data sample with two heavy flavor tagged jets is fitted to templates consisting mainly of $2b$ jet, $2c$ jet, and light flavor jet events, as obtained from ALPGEN+PYTHIA simulated samples. We also compared the shapes of the templates from SHERPA simulated samples and found the templates to be consistent for the two models. Before the fit, all non-Z + jet background contributions, estimated from simulated samples after the MVA$_{bl}$ requirement, are subtracted from the data leaving 180 $Z + 2$ jet events in the combined ee and $\mu\mu$ channel. Next, we measure the jet flavor fractions in the dielectron and dimuon samples combined, yielding the $2b$ jet flavor fraction (f_{bb}) of $0.64 \pm 0.08({\rm stat})$ and the $2c$ jet flavor fraction of $0.32 \pm 0.08({\rm stat})$. Figure 3 shows the one-dimensional projection onto the highest-p_T jet and the second-highest-p_T jet $D_{\rm MJL}$ axis of the two-dimensional fit.

The fraction of $2b$ jets measured in the heavy flavor enriched sample is combined with the corresponding event acceptances to determine the ratio, R, of the cross sections,

$$R = \frac{\sigma(Z + 2b\,{\rm jets})}{\sigma(Z + 2\,{\rm jets})} = \frac{N_{bb} f_{bb}}{N_{\rm incl} \epsilon_{\rm tag}^{bb}} \times \frac{\mathcal{A}_{\rm incl}}{\mathcal{A}_{bb}}, \qquad (1)$$

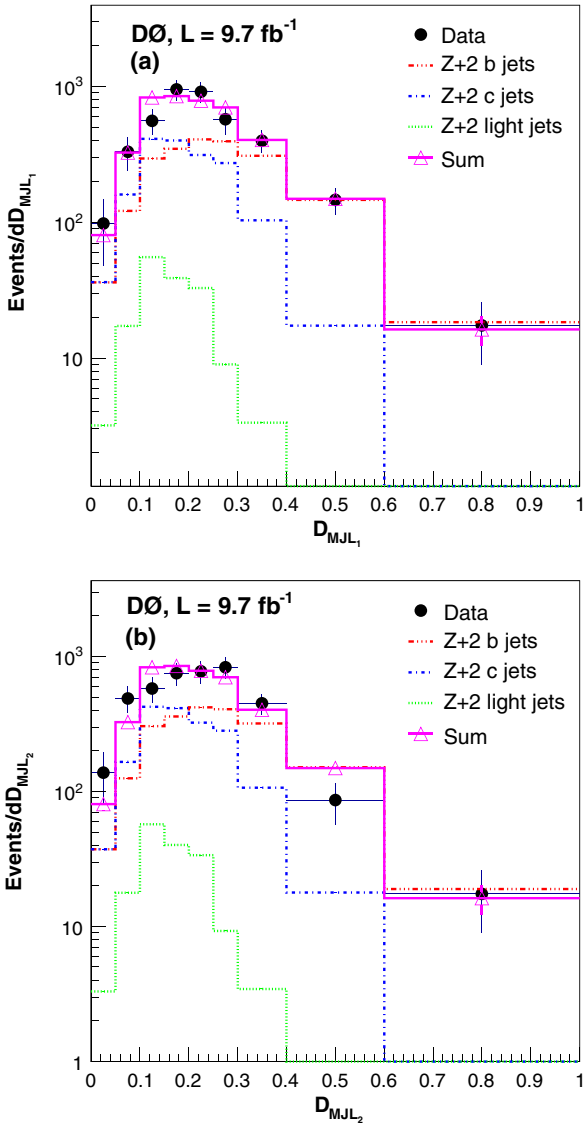

FIG. 3 (color online). The one dimensional projection onto (a) the highest-p_T jet and (b) the second highest-p_T jet $D_{\rm MJL}$ axis of the two-dimensional fit. The distributions of the b, c, and light jets are normalized by the fractions found from the fit.

where $N_{\rm incl}$ is the total number of $Z+2$ jet events before the tagging requirements, N_{bb} is the number of $Z+2$ jet events used in the $D_{\rm MJL}$ fit, f_{bb} is the extracted $2b$ jet fraction, and $\epsilon_{\rm tag}^{bb}$ is the overall selection efficiency of $D_{\rm MJL}$ for $2b$ jets that combines the efficiencies for taggability and MVA$_{bl}$ discriminant. Both $N_{\rm incl}$ and N_{bb} correspond to the number of events that remain after the contributions from non-$Z+$ jets processes have been subtracted from the data.

The pseudorapidity acceptance for electrons and muons is different. In order to quote a combined ratio for the two channels, we correct to a common lepton acceptance as follows. The detector acceptances for the inclusive jet sample and $2b$ jets are determined from MC simulations in the kinematic region that satisfies the p_T and η requirements for leptons and jets. For the $\mathcal{A}_{bb}$ and $\mathcal{A}_{\rm incl}$ calculations, we apply selections for both the electron and muon channels for the fiducial region for the events with two jets and two leptons defined as

$$p_T^{\rm jet} > 20\ {\rm GeV} \quad \text{and} \quad |\eta^{\rm jet}| < 2.5,$$
$$p_T^{\ell} > 15\ {\rm GeV} \quad \text{and} \quad |\eta^{\ell}| < 2. \qquad (2)$$

The resulting ratio of the two acceptances is measured to be $\mathcal{A}_{\rm incl}/\mathcal{A}_{bb} = 1.09 \pm 0.02({\rm stat})$.

Using Eq. (1), we obtain the ratio of the $Z+2b$ jet cross section to the inclusive $Z+2$-jet cross section in the combined $\mu\mu$ and ee channel to be $0.0236 \pm 0.0032({\rm stat})$.

Several systematic uncertainties cancel when the ratio $\sigma(Z+2b\,{\rm jets})/\sigma(Z+2\,{\rm jets})$ is measured. These include uncertainties on the luminosity measurement, lepton trigger efficiency, and lepton and jet reconstruction efficiencies. The remaining uncertainties are estimated separately for the integrated result. The largest systematic uncertainty of 13.7% comes from the uncertainty on the shape of the $D_{\rm MJL}$ templates used in the fit including that due to MC statistics of the samples used to construct the templates. The shape of the templates may be affected by the choice of the b-quark fragmentation function [33], the background estimation, the difference in the shape of the light jet MC template and a template derived from a light jet enriched dijet data sample, and the composition of the charm states used to determine the charm template shape [8]. It also includes uncertainties on production rates of different hadrons and uncertainties on branching fractions. These effects are evaluated by varying the central values by the corresponding uncertainties, one at a time. The entire analysis chain is checked for possible biases using a MC closure test and no significant deviations are observed. The next largest systematic uncertainty of 5.5% is due to the b-jet identification efficiency. The uncertainty on b-jet energy calibration is 2.6%; it comprises the uncertainties on the jet energy resolution and the jet energy scale. For the integrated ratio measurement, these uncertainties, when summed in quadrature, result in a total systematic uncertainty of 14.9%. For the integrated ratio, we obtain

$$R = 0.0236 \pm 0.0032({\rm stat}) \pm 0.0035({\rm syst}). \qquad (3)$$

To check the stability of the result, the ratio is remeasured using a looser(tighter) MVA$_{bl}$ selection with the lower limit on the MVA$_{bl}$ output of $> 0.10 (> 0.225)$. The looser selection provides increased data statistics and the tighter selection yields a $2b$ enriched sample. The new and default ratios are found to be in agreement within uncertainties of about 4%.

To validate the $t\bar{t}$ background estimation, we reduce the contribution of $t\bar{t}$ events by rejecting events where the scalar sum of all jet p_T values is more than 130 GeV. This selection reduces the $t\bar{t}$ fraction by an additional factor of 2 with a signal efficiency of 80%. The new and default ratios are found to be in agreement within systematic uncertainties.

In Table I, we present the ratio of integrated cross sections, $\sigma(p\bar{p} \to Z+2b\,{\rm jet})/\sigma(p\bar{p} \to Z+2\,{\rm jet})$, in the fiducial region defined in Eq. (2). The ratio is compared to predictions from NLO QCD calculations and two MC generators, PYTHIA and ALPGEN. The NLO predictions use the MSTW2008 PDF set [34] using MCFM with central values of renormalization and fragmentation scales $\mu_r = \mu_f = M_Z$. Uncertainties are estimated by varying μ_r and μ_f together by a factor of 2, and are about 15%. ALPGEN generates multiparton final states using tree-level matrix elements. When interfaced with PYTHIA, it employs an MLM scheme [35] to match matrix element partons with those after showering in PYTHIA, resulting in an improvement over leading-logarithmic accuracy. The measured ratio is in reasonable agreement with MCFM NLO calculations considering the uncertainties on the data and theory.

In summary, we report the measurement at the Tevatron of the ratio of integrated cross sections, $\sigma(p\bar{p} \to Z+2b\,{\rm jet})/\sigma(p\bar{p} \to Z+2\,{\rm jet})$, for events with $Z \to \ell\ell$

TABLE I. The ratio of integrated cross sections, $\sigma(p\bar{p} \to Z+2b\,{\rm jet})/\sigma(p\bar{p} \to Z+2\,{\rm jet})$ together with statistical uncertainties ($\delta_{\rm stat}$) and total systematic uncertainties ($\delta_{\rm syst}$). The column $\delta_{\rm tot}$ shows the total experimental uncertainty obtained by adding $\delta_{\rm stat}$ and $\delta_{\rm syst}$ in quadrature. The last three columns show theoretical predictions obtained using NLO QCD with scale uncertainties and two MC event generators, PYTHIA and ALPGEN.

$\sigma(p\bar{p} \to Z+2b\,{\rm jet})/\sigma(p\bar{p} \to Z+2\,{\rm jet})$				
Data $\pm\delta_{\rm stat} \pm \delta_{\rm syst}$	$\delta_{\rm tot}$	NLO QCD(MSTW)	PYTHIA	ALPGEN
$(2.36 \pm 0.32 \pm 0.35) \times 10^{-2}$	0.47×10^{-2}	$(1.76 \pm 0.26) \times 10^{-2}$	2.42×10^{-2}	2.21×10^{-2}

in a restricted phase space of leptons with $p_T^{\ell} > 15$ GeV, $|\eta^{\ell}| < 2.0$ and with two jets limited to $p_T^{\text{jet}} > 20$ GeV and $|\eta^{\text{jet}}| < 2.5$. Measurements are based on the full data sample collected by the D0 experiment in Run II of the Tevatron, corresponding to an integrated luminosity of 9.7 fb^{-1} at a center-of-mass energy of 1.96 TeV. The measured integrated ratio of $0.0236 \pm 0.0032(\text{stat}) \pm 0.0035(\text{syst})$ is in agreement with the theoretical predictions within uncertainties.

We thank John Campbell and Doreen Wackeroth for valuable discussions, and the staffs at Fermilab and collaborating institutions, and acknowledge support from the Department of Energy and National Science Foundation (United States of America); Alternative Energies and Atomic Energy Commission and National Center for Scientific Research/National Institute of Nuclear and Particle Physics (France); Ministry of Education and Science of the Russian Federation, National Research Center "Kurchatov Institute" of the Russian Federation, and Russian Foundation for Basic Research (Russia); National Council for the Development of Science and Technology and Carlos Chagas Filho Foundation for the Support of Research in the State of Rio de Janeiro (Brazil); Department of Atomic Energy and Department of Science and Technology (India); Administrative Department of Science, Technology and Innovation (Colombia); National Council of Science and Technology (Mexico); National Research Foundation of Korea (Korea); Foundation for Fundamental Research on Matter (The Netherlands); Science and Technology Facilities Council and The Royal Society (United Kingdom); Ministry of Education, Youth and Sports (Czech Republic); Bundesministerium für Bildung und Forschung (Federal Ministry of Education and Research) and Deutsche Forschungsgemeinschaft (German Research Foundation) (Germany); Science Foundation Ireland (Ireland); Swedish Research Council (Sweden); China Academy of Sciences and National Natural Science Foundation of China (China); and Ministry of Education and Science of Ukraine (Ukraine).

[1] J. M. Campbell, R. K. Ellis, F. Maltoni, and S. Willenbrock, Phys. Rev. D **73**, 054007 (2006).
[2] F. F. Cordero, L. Reina, and D. Wackeroth, Phys. Rev. D **78**, 074014 (2008).
[3] V. M. Abazov *et al.* (D0 Collaboration), Phys. Rev. Lett. **109**, 121803 (2012); T. Aaltonen *et al.* (CDF Collaboration), Phys. Rev. Lett. **109**, 111803 (2012).
[4] V. M. Abazov *et al.* (D0 Collaboration), Phys. Lett. B **693**, 95 (2010); T. Aaltonen *et al.* (CDF Collaboration), Phys. Rev. Lett. **105**, 081802 (2010).
[5] T. Aaltonen *et al.* (CDF Collaboration), Phys. Rev. D **79**, 052008 (2009).
[6] A. Abulencia *et al.* (CDF Collaboration), Phys. Rev. D **74**, 032008 (2006).
[7] V. M. Abazov *et al.* (D0 Collaboration), Phys. Rev. Lett. **94**, 161801 (2005).
[8] V. M. Abazov *et al.* (D0 Collaboration), Phys. Rev. D **83**, 031105 (2011).
[9] V. M. Abazov *et al.* (D0 Collaboration), Phys. Rev. D **87**, 092010 (2013).
[10] G. Aad *et al.* (ATLAS Collaboration), Phys. Lett. B **706**, 295 (2012).
[11] S. Chatrchyan *et al.* (CMS Collaboration), J. High Energy Phys. 06 (2012) 126.
[12] S. Chatrchyan *et al.* (CMS Collaboration), J. High Energy Phys. 06 (2014) 120.
[13] G. Aad *et al.* (ATLAS Collaboration), J. High Energy Phys. 10 (2014) 141.
[14] V. M. Abazov *et al.* (D0 Collaboration), Nucl. Instrum. Methods Phys. Res., Sect. A **565**, 463 (2006).
[15] M. Abolins *et al.*, Nucl. Instrum. Methods Phys. Res., Sect. A **584**, 75 (2008).
[16] R. Angstadt *et al.*, Nucl. Instrum. Methods Phys. Res., Sect. A **622**, 298 (2010); S. Ahmed *et al.*, Nucl. Instrum. Methods Phys. Res., Sect. A **634**, 8 (2011).
[17] We use a standard right-handed coordinate system. The nominal collision point is the center of the detector with coordinates (0, 0, 0). The direction of the proton beam is the positive $+z$ axis. The $+x$ axis is horizontal, pointing away from the center of the Tevatron ring. The $+y$ axis points vertically upwards. The polar angle, θ, is defined such that $\theta = 0$ is the $+z$ direction. The rapidity is defined as $y = -\ln[(E + p_z)/(E - p_z)]$, where E is the energy and p_z is the momentum component along the proton beam direction. Pseudorapidity is defined as $\eta = -\ln(\tan\frac{\theta}{2})$. φ is defined as the azimuthal angle in the plane transverse to the proton beam direction. Also, η_{det} and ϕ_{det} are the pseudorapidity and the azimuthal angle measured with respect to the center of the detector.
[18] S. Abachi *et al.* (D0 Collaboration), Nucl. Instrum. Methods Phys. Res., Sect. A **338**, 185 (1994).
[19] The primary $p\bar{p}$ interaction vertex is that found to be the most likely collision point, among possibly several collisions within a specific beam crossing, from which selected objects emanate. The algorithm for defining it can be found in [20].
[20] V. M. Abazov *et al.* (D0 Collaboration), Nucl. Instrum. Methods Phys. Res., Sect. A **763**, 290 (2014).
[21] V. M. Abazov *et al.* (D0 Collaboration), Nucl. Instrum. Methods Phys. Res., Sect. A **737**, 281 (2014).
[22] G. C. Blazey *et al.*, arXiv:hep-ex/0005012.

[23] V. M. Abazov *et al.* (D0 Collaboration), Nucl. Instrum. Methods Phys. Res., Sect. A **763**, 442 (2014).
[24] T. Sjöstrand, S. Mrenna, and P. Skands, J. High Energy Phys. 05 (2006) 026. Version 6.409 with Tune A was used.
[25] M. L. Mangano, F. Piccinini, A. D. Polosa, M. Moretti, and R. Pittau, J. High Energy Phys. 07 (2003) 001. Version 2.11 was used.
[26] J. Pumplin, D. Robert Stump, J. Huston, H.-L. Lai, P. Nadolsky, and W.-K. Tung, J. High Energy Phys. 07 (2002) 012.
[27] J. M. Campbell and R. K. Ellis, Phys. Rev. D **60**, 113006 (1999); **62**, 114012 (2000); **65**, 113007 (2002).
[28] U. Langenfeld, S. Moch, and P. Uwer, Phys. Rev. D **80**, 054009 (2009).
[29] V. M. Abazov *et al.* (D0 Collaboration), Phys. Rev. Lett. **100**, 102002 (2008).
[30] R. Brun and F. Carminati, CERN Program Library Long Writeup W5013 (1993).
[31] A. Hoecker *et al.*, TMVA: Toolkit for Multivariate Data Analysis, *Proc. Sci.*, ACAT2007 (2007) 040.
[32] V. M. Abazov *et al.* (D0 Collaboration), Phys. Lett. B **718**, 1314 (2013).
[33] V. M. Abazov *et al.* (D0 Collaboration), Phys. Rev. D **84**, 032004 (2011).
[34] A. D. Martin, W. J. Stirling, R. S. Thorne, and G. Watt, Eur. Phys. J. C **63**, 189 (2009).
[35] F. Caravaglios, M. L. Mangano, M. Moretti, and R. Pittau, Nucl. Phys. **B539**, 215 (1999).